Applied Geochemistry 105 (2019) 45–54

Contents lists available at ScienceDirect

Applied Geochemistry

journal homepage: www.elsevier.com/locate/apgeochem

Radium retention by blended cement pastes and pure phases (C-S-H and C-A-S-H gels): Experimental assessment and modelling exercises

J. Olmeda[a,*], T. Missana[b], F. Grandia[a], M. Grivé[a], M. García-Gutiérrez[b], M. Mingarro[b], U. Alonso[b], E. Colàs[a], P. Henocq[c], I. Munier[c], J.C. Robinet[c]

[a] Amphos 21 Consulting S.L., C/ Veneçuela 103, 08019, Barcelona, Spain
[b] CIEMAT, Physical Chemistry of Actinides and Fission Products Unit, Department of Environment, Avenida Complutense 40, 28040, Madrid, Spain
[c] Andra, 1/7 rue Jean Monnet, Parc de la Croix Blanche, 92298, Châtenay-Malabry Cedex, France

ARTICLE INFO

Editorial handling by Dr D A. Kulik

Keywords:
Radium
Radionuclide
Adsorption
Cement
C-S-H
C-A-S-H

ABSTRACT

Cementitious materials are planned to be used in current designs of geological disposal of radioactive waste. Their main function is the structural reinforcement, but they could contribute to the retention of some radionuclides via adsorption and/or precipitation. In this work, a set of laboratory experiments has been performed to determine the capacity of blended cement (CEM V/A) containing fly ash (FA) and blast furnace slag (BFS) to adsorb radium. The study has focused on the hydrated cement paste (HCP) with different degradation states and on cement representative pure phases (C-S-H and C-A-S-H at variable Ca/Si and Al/Si ratios). The experimental results show that retention of Ra by hydrated cements is high; C-S-H and C-A-S-H phases were proven to be very relevant in Ra uptaking, with log Kd up to 4.2 and 5.1, respectively. The adsorption of radium into these phases is interpreted to be driven by surface complexation on weak and strong silanols-like sites and ionic exchange with Ca. Since Ra adsorption has been proven to be inversely proportional to dissolved Ca content, an enhanced adsorption capacity of the cementitious hydrates (C-S-H phases) is expected as degradation of cement proceeds.

1. Introduction

The French National Radioactive Waste Agency (Andra) is currently developing disposal concepts for low-level long-lived (LL-LL) residues, including technologically enhanced naturally occurring radioactive materials (TENORM), such as Ra-bearing waste from REE and Th industrial production in France (Andra, 2012). One of these types of radioactive wastes consists mainly of radiobarite ($(Ba,Ra)SO_4$), a granular material stored in drums, in which ^{226}Ra is the most abundant radioisotope (half-life = 1,600 years). Ra activities are up to 200 $Bq{\cdot}g^{-1}$ which exceeds the International Basic Safety Standards threshold of 1 $Bq{\cdot}g^{-1}$ for TENORM materials (International Atomic Energy Agency, 2011); therefore, radiological protection plans need to be implemented.

Underground repositories have emerged as the safest option for the definitive disposal of the aforementioned type of radwaste. The construction and closure of these repositories would include, largely, the use of cementitious materials. In addition to their structural properties, cement-based materials exhibit radionuclide adsorption capacities (Atkins and Glasser, 1992; Evans, 2008) that would help reduce their mobilities. Studies on the adsorption of Ra on hardened cement pastes (HCP) or pure cement phases are relatively scarce (Holland and Lee, 1992; Bayliss et al., 2000; Tits et al., 2006a, b; Lange et al., 2018). Conventionally, it is assumed that the geochemical behaviour of Ra is similar to that of Sr or Ba, which are considered analogue elements.

The assessment of the retention properties of cementitious materials in a disposal site must consider the chemical changes of these materials, which are due to the interactions with ground water, especially given the long disposal period required for radwaste, during which cement-based materials undergo gradual degradation. Consequently, comprehensive adsorption evaluation requires investigating different degradation states. Cement alteration starts with the removal of alkali hydroxides, followed by the dissolution of portlandite, and the decalcification and dissolution of hydrated silicate and aluminate phases (Adenot, 1992; Taylor, 1997; Wang et al., 2010; Olmeda et al., 2017). With variable chemical compositions ($xCaO{\cdot}SiO_2{\cdot}yH_2O$ with approx. $0.6 < x < 1.8$), calcium-silicate-hydrate (C-S-H) gels are the most important hydration products of cement. Due to their large specific surface areas, they have strong potentials for ion adsorption (Atkins and Glasser, 1992; Evans, 2008; Olmeda et al., 2017; Aggarwal et al., 2000). Furthermore, cation uptake into the C-S-H structure by ion-exchange processes may be significant under some conditions (Tits et al., 2006a,

* Corresponding author.
E-mail address: javier.olmeda@amphos21.com (J. Olmeda).

https://doi.org/10.1016/j.apgeochem.2019.04.004
Received 14 January 2019; Received in revised form 26 March 2019; Accepted 4 April 2019
Available online 09 April 2019
0883-2927/

b; Beaudoin et al., 1990; Richardson and Groves, 1993; Pointeau et al., 2004; Papadokostaki and Savidou, 2009).

Blended cements like CEM V could be suitable for constructing the repository, owing to their enhanced mechanical property and high sulfate resistance compared with those of CEM I. These cements often contain substantial amounts of Al which could improve the formation of Al-bearing phases, such as strätlingite, hydrogarnet, or other hydrated calcium aluminates. Al can also be incorporated into the C-S-H structures, forming so-called C-A-S-H (calcium-aluminate-silicate-hydrate) phases with different structures and higher chain lengths than those of C-S-H (Sun et al., 2006; Lothenbach et al., 2011; Lodeiro et al., 2010; L'Hôpital et al., 2015). Some dedicated studies have shown that C-A-S-H gels may have higher adsorption capacities for Cs, Sr, and alkali compared to those of C-S-H (Li and Pang, 2014; Hong and Glasser, 2002). However, the retention capacities for other bivalent cations, especially for Ra, are not well known and must therefore be studied.

The objective of this work is to gain better understanding of Ra adsorption on cement-based materials and to assess the adsorption capacities at different degradation states. Furthermore, the roles of the main cementitious phases (C-(A)-S-H) on Ra retention is studied and compared. This contribution is based on in-depth experimental studies consisting of kinetic tests and adsorption isotherms on hardened cement pastes at different degradation states as well as on pure cement phases, such as C-S-H and C-A-S-H with different Ca/Si and Al/Si ratios. The mechanisms governing the binding of Ra onto these phases are described by numerical modelling exercises that accurately fit the experimental data.

2. Materials and methods

2.1. Preparation of hardened cement pastes

Cement-type CEM V/A(S-V) was employed in this study; it contains equal concentrations (23 wt% of the total mass content) of fly ash (FA) and blast furnace slag (BFS). The chemical and mineralogical compositions provided by the manufacturer (*Ciments Calcia*) are shown in Table 1.

Samples of ∅ 4 × 10 cm hydrated cement (HCP) were prepared with deionised, degassed Milli-Q water (DDW) with a water-cement ratio of 0.4. After 28 days of curing at 98% RH, the HCP samples were ground and sieved to a particle size below 63 µm (BET-N_2 area = 16.2 m^2/g).

The degradation of HCP to state II (alkali-free condition) was achieved by leaching the sieved HCP sample in DDW at a solid-liquid (S/L) ratio of 12.5 g/L for 15 days under continuous stirring (Pointeau et al., 2004). The procedure was carried out in HDPE bottles, inside a glovebox, under controlled temperature (25 ± 2 °C) and N_2 atmosphere (CO_2 < 10 ppm and O_2 < 1 ppm). After the reaction, HCP suspensions were passed through a nylon filter (0.22 µm mesh opening) using a Büchner funnel. The leached HCP was dried in the same Büchner funnel with acetone and was placed in airtight 25 mL vials.

Cementitious pore waters were analysed by ICP-OES (*VARIAN 735ES*) and ionic chromatography (*DIONEX ICS-2000*); pH measurements were recorded using a pH-meter (*Mettler Toledo - S220*) with a solid polymeric electrode (*Xerolyt*). The compositions of the crystalline and semi-crystalline phases in the solid HCP samples were determined with an X-ray diffractometer (*PANalytical X'Pert PRO MPD Alpha1* with Cu/W X-ray generator working at 40 kV and 40 mA).

2.2. Synthesis of C-S-H gels

C-S-H phases with variable Ca/Si ratios were synthesised following the methodology proposed by Pointeau (2000). Reagent grade CaO (Alfa-Aesar 99.95% purity) and silica fume (Aldrich 99.8% purity) were hydrated with DDW in HDPE dark containers, at different weight proportions to obtain 1 L suspensions with four incremental Ca/Si molar ratios (i.e. 0.8, 1.0, 1.2, and 1.6), and a S/L ratio of 10 g/L. An additional C-S-H sample with a Ca/Si ratio of 0.8 was synthesised (S/L = 20 g/L).

All the suspensions were placed inside the glovebox under N_2 atmosphere and under continuous stirring (CO_2 < 10 ppm and O_2 < 1 ppm) to prevent carbonation processes and to promote a homogeneous reaction, respectively. The periods of time needed to attain equilibrium in the C-S-H samples varied between a few days and several months depending on the nature of the initial reagents, and the change in the concentration of the solution (Taylor, 1950). Therefore, conductivity (*Crison EC Meter Basic 30*$^+$) and pH (*Mettler Toledo - S220*) were periodically monitored until a steady-state was attained.

The mother solution was separated from the solid by filtration with a nylon filter (mesh opening of 0.1 µm), and aqueous Ca and Si contents were analysed by ICP-OES. The solid samples were dried to constant weights, and the specific surface areas were determined by BET-N_2 analyses. The Ca/Si ratios in the solid samples as well as their distribution were determined by (micro) proton induced X-ray emission (µPIXE). The surface charges (ζ-potential) of the synthesised C-S-H gels were measured by laser Doppler electrophoresis (*Malvern Zetamaster* with 5-mW He–Ne laser, Missana et al., 2017).

2.3. Synthesis of C-A-S-H gels

The C-A-S-H phases were synthetized by mixing reagent grade CaO (Alfa Aesar 99.95% purity), silica fume (Aldrich 99.8% purity), and Al$(NO_3)_3{\cdot}9H_2O$ (Sigma Aldrich), at different weight proportions with DDW to obtain suspensions of S/L = 10 g/L, with variable Ca/Si ratios. Al/Si molar ratios were up to 0.20, in accordance with literature values to avoid the precipitation of other Al-containing phases (Sun et al., 2006; Pardal et al., 2009; L'Hôpital et al., 2016). The suspensions were continuously stirring in HDPE dark containers inside the glovebox, under controlled temperature (25 ± 2 °C) and N_2 atmosphere (CO_2 < 10 ppm and O_2 < 1 ppm) to induce a homogeneous reaction and prevent carbonation. The conductivity and pH were monitored daily until a steady-state was attained. The solids were separated from the liquid by filtration using 0.1 µm nylon filters, after which they were left to dry inside the glovebox. The dessication process was controlled by periodic weighting until constant masses were achieved. The average Ca/Si and Al/Si ratios in the solids were determined by XRF (*Axios Advanced Panalytical*). The pH and concentrations of Ca, Si, and Al were determined in the liquid fraction. Surface charges (ζ-potential) were measured by laser Doppler electrophoresis.

2.4. Radionuclide and counting techniques

For the investigation of Ra adsorption onto cementitious materials, a $^{226}Ra(NO_3)_2$ standard solution in 1 M HNO_3 was used (*Eckert and Ziegler Isotope Products*). The stock solution has an activity of 2 µCi/mL (7.4×10^4 Bq/mL), equivalent to a Ra concentration of 8.85×10^{-6} M, and contains a carrier of stable Ba (10 µg/mL solution, i.e.

Table 1
Chemical and mineralogical compositions of CEM V/A(S-V).

Chemical compositions	SiO_2	Al_2O_3	Fe_2O_3	TiO_2	MnO	CaO	MgO	SO_3	K_2O	Na_2O	P_2O_5
wt.%	29.4	10.2	3.3	0.5	0.2	47.3	2.7	2.9	1.42	0.23	0.2
Mineralogical compositions	C_3S	C_2S	C_3A	C_4AF							
wt.%	67	12	11	7							

7.28×10^{-5} M).

Herein, liquid scintillation counting (LSC) was selected for the ^{226}Ra measurement due to its high efficiency. An *alpha-beta* 2700 TR LSC was used with a *Beckman Insta-Gel Plus TM* scintillation cocktail, suitable for counting samples in broad pH and ionic strength ranges.

The ^{226}Ra measurements required an average in-growth time of 22 days (approx. six half-lives of its main daughter, i.e. ^{222}Rn); consequently, the samples were hermetically sealed to avoid ^{222}Rn leakage and to ensure secular equilibrium between the gas and its progeny.

2.5. Adsorption experiments

Standard batch adsorption experiments were conducted on hydrated cement and pure phase suspensions inside a glovebox, under N_2 atmosphere (CO_2 < 10 ppm and O_2 < 1 ppm) and at T = 25 ± 2 °C. The HCP (states I and II) samples were ground and sieved to a particle size below 63 µm and were put in contact with the corresponding pore water with a S/L ratio of 10 g/L. Similarly, adsorption tests were done in discrete vials where the C-S-H or C-A-S-H phases were put in contact with their respective mother solutions resulting from the synthesis at a S/L ratio of 10 g/L. Additionally, tests at a S/L ratio of 20 g/L were conducted with the C-S-H samples which have a Ca/Si ratio of 0.8.

Once equilibrium was attained, the suspensions were spiked with the ^{226}Ra stock solution to a total radionuclide concentration ranging from 8×10^{-10} to 2.5×10^{-8} M (6.69–209 Bq/mL). The adsorption kinetics were initially determined to calculate the equilibrium time. The samples were continuously stirred for periods between 3 and 94 days. After the reaction, solid and liquid fractions were separated by centrifugation at 25,000 × *g* for 30 min (*JOUAN MR23i*). The activity of aqueous Ra was analysed in triplicate from each collected supernatant; the final pH of the solution was also recorded.

Once the appropriate adsorption duration had been selected, adsorption isotherms were performed with varying radionuclide concentrations. The same procedure as in adsorption kinetic tests was used for measuring the Ra concentration in the liquid fraction.

Ra uptake is reported as distribution coefficient, K_d (L/kg), which represents the degree of adsorption; it is defined as the ratio of the element mass (activity) per mass unit of the solid, to the mass (activity) per volume unit of the solution (Eq. (1)).

$$K_d = \frac{[Ra]_0 - [Ra]_{eq}}{[Ra]_{eq}} \cdot \frac{V}{m}. \quad (1)$$

Where $[Ra]_0$ and $[Ra]_{eq}$ are the initial and final concentrations of Ra in Bq/mL, respectively; *m*, the mass (kg) of the adsorbent material; and *V (L)*, the volume of the liquid fraction. The associated uncertainties were calculated using the standard deviation from three replicates.

3. Results

3.1. Material characterisation

3.1.1. Characterisation of hardened cement pastes

Generally, a sound HCP (State I) pore-water composition is characterised by dissolved high alkali (Na + K) content, which maintains the pH of the system at values above 13 (Table 2).

The chemistry of the cementitious pore waters tends to evolve with the curing time; therefore, slightly different concentrations were observed with HCPs cured at comparatively long periods, especially in terms of alkali contents (Hong and Glasser, 2002, 1999; Chen and Brouwers, 2010). Once the alkalis have been leached out from the system (State II), an increase in Ca concentration is observed with respect to portlandite solubility (Pointeau et al., 2006). The pH of the degraded HCP pore water was 12.2 (Table 2) which indicates the dissolution of portlandite (pH ≈ 12.45 at equilibrium with portlandite), while alkali concentration remained at 8.5×10^{-3} mol/L.

Table 2
Analysed composition of the fresh (state I) and degraded (state II) HCP pore waters.

Composition	Sound HCP (State I) pore water (mol/L)	Degraded HCP (State II) pore water (mol/L)
pH	13.2	12.2
Al	4.08×10^{-6}	$< 1.11 \times 10^{-6}$
Ba	2.84×10^{-6}	8.01×10^{-6}
Ca	7.49×10^{-4}	5.07×10^{-3}
Cl	4.23×10^{-4}	6.77×10^{-4}
Fe	$< 5.37 \times 10^{-7}$	$< 5.37 \times 10^{-7}$
K	1.98×10^{-1}	6.39×10^{-3}
Mg	$< 1.23 \times 10^{-6}$	$< 1.23 \times 10^{-6}$
Na	8.16×10^{-2}	2.17×10^{-3}
Si	3.83×10^{-5}	1.25×10^{-5}
S(VI)	1.41×10^{-3}	7.60×10^{-6}

Consequently, the measured Ca concentration of the degraded HCP pore water (5.07×10^{-3} mol/L) could correspond to its concentration in C-S-H with a high Ca/Si ratio, i.e. 1.2 < Ca/Si < 1.5, in equilibrium with the measured alkali concentration.

The XRD pattern of the sound HCP sample showed the presence of portlandite (CH, main peaks in blue in Fig. 1), with other standard hydration products of a BFS/FA blended cement, e.g. ettringite (AFt-SO_4), monosulfo-aluminate (AFm-SO_4), and hydrogarnet (HG). Broad signals of poorly crystallized C-S-H phases were observed overlapping the peaks corresponding to anhydrous compounds at 29-30° and 32-33° 2θ (Taylor, 1997; Grangeon et al., 2013).

The XRD pattern of the degraded HCP sample (in orange in Fig. 1) seemed to be similar to that of the sound HCP sample, except for the absence of peaks corresponding to portlandite. As observed from the pore water composition and XRD patterns, the degraded HCP sample corresponds more to a state III degraded HCP without portlandite and with a poorly decalcified C-S-H, than to a state II, as commonly defined (Adenot, 1992; Taylor, 1997; Olmeda et al., 2017; Ochs et al., 2016).

3.1.2. Characterisation of C-S-H gels

The analyses of both aqueous and solid phases of the synthesised C-S-H gels are shown in Table 3. Ca and Si were homogeneously distributed across the sample, and the measured Ca/Si ratio agrees with

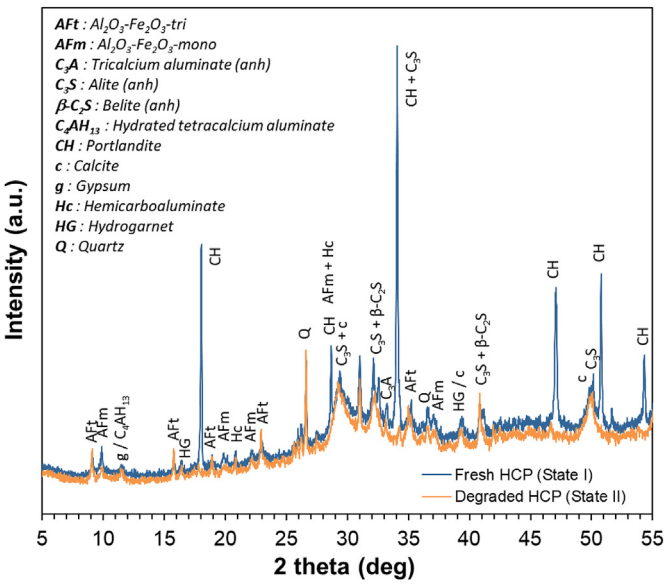

Fig. 1. X-ray diffraction spectra of the HCP samples: Sound (state I - blue line); Degraded (state II - orange line). (For interpretation of the references to colour in this figure legend, the reader is referred to the Web version of this article.)

Table 3
Analyses of the aqueous and solid fractions of the synthesised C-S-H gels.

	Aqueous			*Solid*		
C-S-H (Ca/Si ratio) sample 10 g/L	Ca (M)	Si (M)	pH	Ca/Si ratio (μPIXE)	BET-N_2 (m^2/g)	ζ-potential (mV)
C-S-H (0.8)	1.10×10^{-3}	1.25×10^{-3}	10.38	0.89 ± 0.04	200 ± 3	−12.1 ± 0.6
C-S-H (1.0)	2.05×10^{-3}	6.66×10^{-5}	11.41	1.03 ± 0.04	124 ± 2	−3.0 ± 0.4
C-S-H (1.2)	5.09×10^{-3}	2.50×10^{-5}	12.19	1.26 ± 0.15	109 ± 2	4.1 ± 0.3
C-S-H (1.6)	1.50×10^{-2}	3.33×10^{-6}	12.37	1.60 ± 0.11	73 ± 1	11.8 ± 1.5

the targeted value, confirming the reliability of the synthesis procedure followed. The measured BET surface areas decreased in the C-S-H gels as the Ca/Si ratios increased, in agreement with trends from other studies (Pointeau, 2000; Trapote-Barreira et al., 2014; Roosz et al., 2018). The zeta potential increased with Ca concentration and pH in the equilibrium solution (Table 3).

SEM and EDX images of the C-S-H gels are shown in Fig. 2. The Ca and Si semi-quantitative EDX analyses agreed with the theoretical Ca/Si ratios expected in the different C-S-H phases studied.

As shown in Fig. 3a–c, Ca and Si concentrations as well as the pH of the equilibrium solution at different molar Ca/Si ratios agreed with the data reported in the literature (Pointeau, 2000; Taylor, 1950; Atkins et al., 1992; Chen et al., 2004; Cong and Kirkpatrick, 1996; Flint and Wells, 1934; Glasser et al., 1999; Greenberg and Chang, 1965; Grutzeck et al., 1989; Haas, 2012; Henocq, 2005; Sugiyama, 2008; Walker et al., 2007, 2016).

3.1.3. Characterisation of C-A-S-H gels

The analyses of the C-A-S-H supernatants indicated that Al was removed from the solution (above 99.5% of its initial concentration) (Table 4). The percentages of Al incorporated into the C-S-H gels were higher in the samples with lower Ca/Si ratios than in the samples with higher Ca/Si ratios (removal of 99.9% of the initial Al content from the solution). This agrees with other studies where comparatively high Al affinities were reported for C-S-H samples with a low Ca/Si ratio (0.8) (Richardson and Groves, 1993; L'Hôpital et al., 2016; Faucon et al., 1999). Different substitution mechanisms account for such behaviour, i.e. tetrahedral coordination (Al(IV)) at low Ca/Si ratios, and pentahedral (Al(V)) and/or octahedral (Al(VI)) coordination at high ratios (Sun et al., 2006; L'Hôpital et al., 2015; Faucon et al., 1999; Pardal et al., 2012). The substitution capacities of these latter co-ordinations are limited and correspond to amorphous aluminium hydroxides or to calcium aluminate hydrates at either the C-S-H surface or the interlayer sites (Faucon et al., 1999; Andersen et al., 2006; Renaudin et al., 2009). The Al/Si ratio obtained by XRF in the solid was consistent with the initial aqueous composition; consequently, the Ca/Si ratio was lower than its starting ratio (Table 4). This fact was consistent with the analysed Ca concentration.

3.2. Results of the adsorption experiments

3.2.1. Hardened cement pastes

Ra uptake onto the HCP samples followed a logarithmic function attaining equilibrium after 14 days. Linear adsorption isotherms were obtained in state I and II HCP suspensions (Fig. 4), showing that radionuclide adsorption was (i) constant within the Ra concentration range studied and (ii) far from reaching surface site saturation. A slightly lower adsorption capacity was observed for Ra in the degraded HCP compared to that in the sound HCP, with respective log K_d values of 2.69 ± 0.01 and 2.77 ± 0.02 (Table 5).

3.2.2. C-S-H gels

Ra adsorption onto the C-S-H phases followed a logarithmic function with rapid adsorption within few days; sorption equilibrium was attained after roughly 10 days. Ra adsorptions for all the samples studied appeared to follow the Langmuir-type isotherm, and the sites seemed to attain saturation at high Ra concentrations (Fig. 5). The affinity for Ra decreased as the Ca/Si ratio increased, i.e. with the increase in pH and aqueous Ca concentration in solution (section 5). No significant difference was observed between the two different S/L ratios studied, and the variability of the K_d values was within the range of uncertainty. The obtained log K_d values are summarised in Table 5.

3.2.3. C-A-S-H gels

The Ra adsorption on the C-A-S-H samples proceeded fast; therefore, the overall contact time adopted for the adsorption isotherms was also set to 10 days. A general strong retention of Ra by the C-A-S-H gels was observed with dependency on the Al/Si ratio. According to the results (Fig. 6), Ra uptake increased as follows:

C-A-S-H (0.8–0.05) ~ C-A-S-H (1.2–0.05) < C-A-S-H (0.8–0.20) < C-A-S-H (1.2–0.20)

Increased Ra retention was obtained with samples of relatively high Al/Si ratios. At equal Al/Si ratios, the distribution coefficients were high for the C-A-S-H samples with high Ca/Si ratios. These results are comparable to those obtained from the C-S-H phases (Fig. 5 and Table 5), i.e. at low Al/Si ratios, Al incorporation into the C-S-H structure does not seem to have a significant influence on the Ra uptake. When the degree of Al substitution increases (high Al/Si ratio), the retention capacities of the C-A-S-H gels increase compared to the retention capacities of the C-S-H gels with equivalent Ca/Si ratios; however, this increase is only significant in the samples with a high Ca/Si ratio (1.2).

4. Modelling approach for Ra adsorption data

The data obtained in this work from the adsorption studies with C-S-H gels were modelled following the diffuse double layer model (DLM) reported in Missana et al. (2017). The calculations were performed at 25 °C using the geochemical code PhreeqC v.3.3.3 (Parkhurst and Appelo, 2013), and the ThermoChimie v.9.0.b database (Giffaut et al., 2014; www.thermochimie-tdb.com). The mechanisms considered to model the experimental adsorption data are outlined below.

i. Diffuse Double Layer Surface-Complexation Model
   a) Weak silanol sites $Si_{we}O$-
      - Protonation/deprotonation
      - Ra, Ba, and Ca complexation
   b) Strong silanol sites $Si_{st}O$-
      - Protonation/deprotonation
      - Ra and Ba complexation
ii. Cation exchange model, X_2Ca

In the model, the retention of alkaline-earth cations is governed by surface complexation on *weak* and *strong* silanol-like sites; ionic exchange with Ca is included (Lange et al., 2018). These two mechanisms have been suggested in analogy with those expected in clays, as some structural similarities (layered structure and silanol groups) can be established for both solid types. In clayey systems, sorption at a low pH and in a low-ionic strength media is suggestively dominated by cation

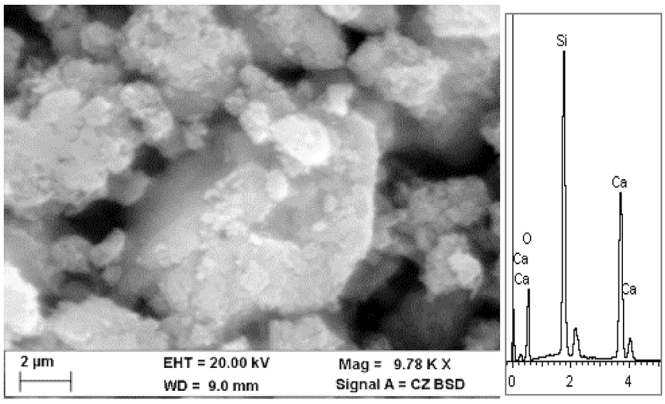

(a)

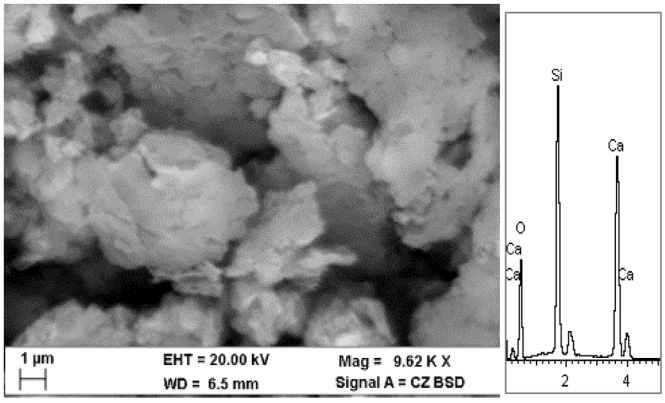

(b)

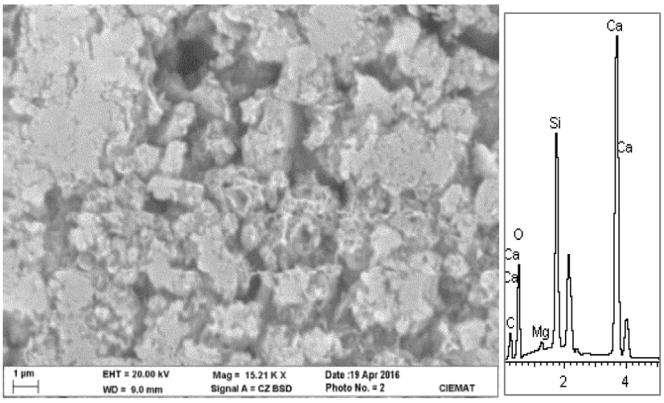

(c)

Fig. 2. SEM-SEI micrographs and EDX analyses of the synthesised C-S-H phases (a) Ca/Si = 0.8; (b) Ca/Si = 1.2; (c) Ca/Si = 1.6.

exchange processes (Tournassat et al., 2013). In contrast, sorption at high pH values (as in the present case) could be dominated by sorption in either high or low energy sites for low or high metal concentrations, respectively.

Note that the competition between Ra and Ba was considered in the calculations, since Ba is present in the experiments as a carrier of the Ra stock solution (section 2.4).

4.1. Surface-complexation

Under alkaline conditions, silanol groups are deprotonated according to Eq. (2). The intrinsic equilibrium constant associated with this reaction can be described using Eq. (3), where {} is the ionic activity, and () is the ion concentration. The activity coefficients for the surface species are all assumed to be 1. The exponential represents the coulombic term that accounts for the electrostatic effects; where Ψ is the surface potential; R, the molar gas constant; and T, the temperature.

$$SiOH \Leftrightarrow SiO^- + H^+. \quad (2)$$

$$K = \frac{[SiO^-]\{H^+\}}{[SiOH]} \exp\left(-\frac{F\Psi}{RT}\right). \quad (3)$$

Following the model in Missana et al. (2017), the acid-base equilibrium constant of the C-S-H silanol groups (Eq. (2)) used in this work is log K = 6.8 ± 0.5 (Papirer, 2000). The total numbers of adsorption sites for each C-S-H were calculated from BET values assuming densities of 13 and 3.5×10^{-3} µmol/m^2 for weak and strong sites, respectively (Missana et al., 2017). These values are of the same order of magnitude relative to those used in Pointeau et al. (2001) and Ochs et al. (2006). The parameters used in this work are listed in Table 6.

4.2. Cation exchange

The model for Ra retention includes cation exchange, where Ra^{2+} exchanges with Ca^{2+} at the C-S-H surface according to Eq. (4). This mechanism has already been suggested for Ra retention in cement phases (Tits et al., 2006a). The selectivity coefficient for the exchange reaction is defined by Eq. (5).

$$X_2Ca + Ra^{2+} \Leftrightarrow X_2Ra + Ca^{2+} \quad (4)$$

$$^{Ra}_{Ca}K_C = \frac{N_{Ra}\,[Ca^{2+}]}{N_{Ca}\,[Ra^{2+}]} \quad (5)$$

Where $N_M{}^{2+}$ is the ionic equivalent fractional occupancy which can be expressed by $N_M{}^{2+} = 2*\{M^{2+}\}/CEC$; $\{M^{2+}\}$, the amount of divalent cation adsorbed (mol/kg); and CEC, the cation exchange capacity of the material (eq/kg).

All the parameters used in the model are summarised in Table 6, and the modelling results are shown in Fig. 7 (dash-dotted lines). In general, the approach used (surface complexation and cation exchange) in the model can reproduce the experimental data with high accuracy.

5. Discussion

The chemistry of Ra under high pH conditions is governed by $RaOH^+$ and, mainly, Ra^{2+}. $RaSO_4$(aq) may also be present in sulfate concentration (~1 mM), with precipitation of $RaSO_4$(s) at high concentrations and very high Ra activity. This aqueous speciation drives the Ra-binding mechanisms in cementitious materials, which are thought to be similar to Ca (Evans, 2008; Tits et al., 2006a; Ochs et al., 2016). The influence of aqueous Ca content over Ra adsorption is evident (Fig. 8), as the Ra distribution coefficients depend on the Ca/Si ratio and decrease with increasing Ca concentration. This behaviour is linked to the C-S-H surface charge, i.e. a decrease in Ra retention is a consequence of the decrease in the number of negatively charged silanol groups available for Ra adsorption. Atkins and Glasser (1992) showed that the C-S-H phases with higher Ca/Si ratios exhibited better iodine adsorption relative to those with lower ratios. Several authors (Tits et al., 2006a, b; Hong and Glasser, 1999; Lange et al., 2018; Bach et al., 2013; Henocq, 2017; Viallis-Terrisse, 2000, 2001) observed that the C-S-H phases with low Ca/Si ratios are expected to be good sorbents for cationic species. As the zeta-potential values of the C-S-H gels tend to decrease with the pH or Ca concentration of the pore water, two equilibria were proposed to drive the evolution of the C-S-H surface

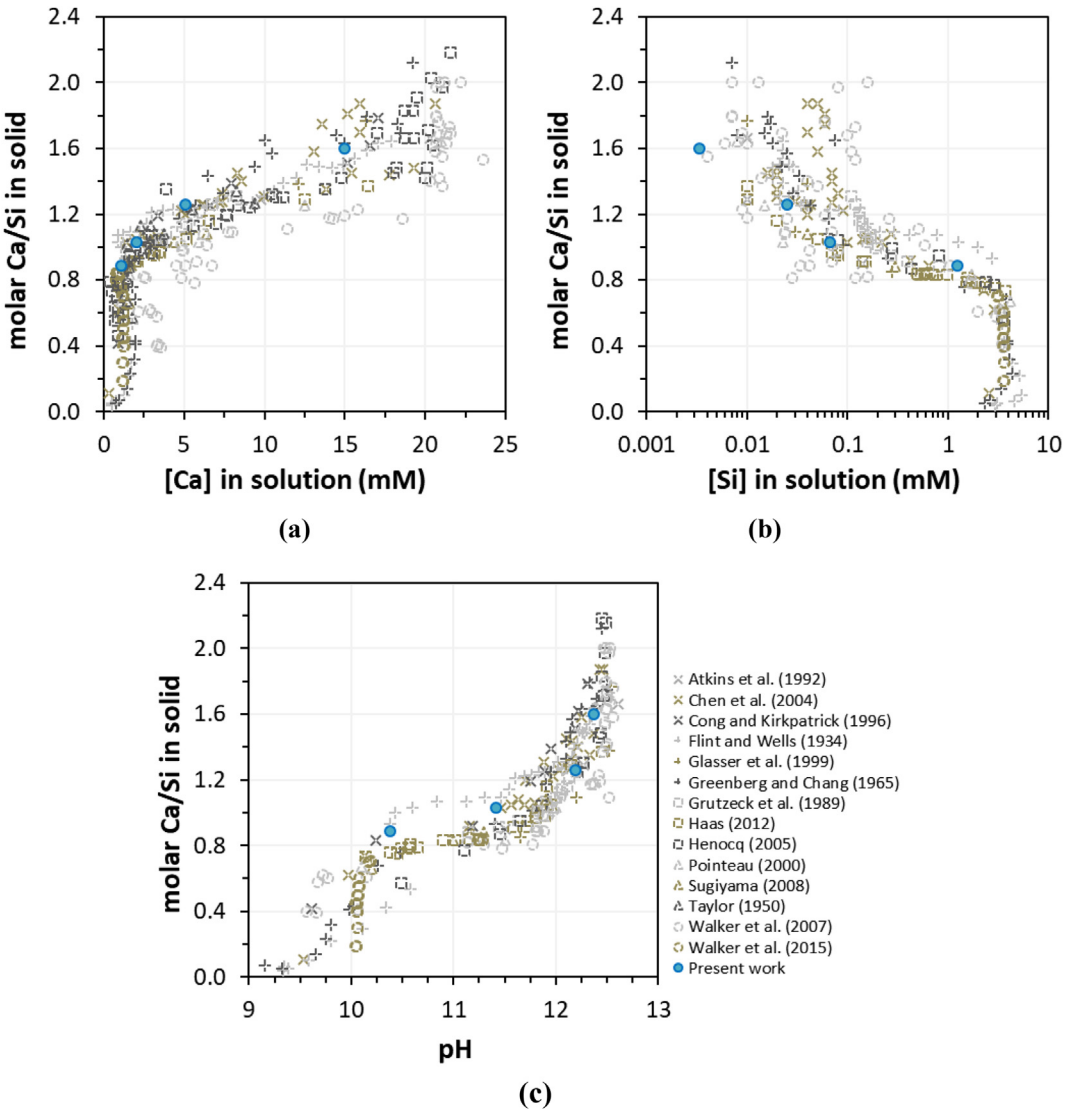

Fig. 3. Diagrams showing the molar Ca/Si ratios in C-S-H gels against the total aqueous Ca (a) and Si (b) concentrations (mM); pH of the solution at equilibrium (c). Relevant data available in the literature have also been included for comparison. Note that there are some data at different temperatures (e.g. Greenberg and Chang, 1965 at 50 °C; Taylor, 1950 at 17–20 °C; Flint and Wells, 1934 at 30 °C) or produced by other methods, such as C_3S dissolution or double decomposition (Taylor, 1950; Chen et al., 2004).

chemistry (Pointeau, 2000; Viallis-Terrisse et al., 2001): ionization of silanol sites, mostly through deprotonation (Eq. (6)), and Ca^{2+} sorption on the silanol sites (Eq. (7)).

$$> SiOH \rightarrow > SiO^- + H^+ \quad (6)$$

$$> SiOH + Ca^{2+} \rightarrow > SiOCa^+ + H^+ \quad (7)$$

A number of studies have focused on Ra solubility and adsorption onto cement pastes. In the review carried out by Ochs et al. (2016), which included the work of Tits et al. (2006a), they established upper and lower limits and proposed 300 and 100 L/kg as the best estimate values for sound (state I) and degraded (state II) HCP, respectively. The adsorption values obtained in this work for analogue conditions are 583 and 492 L/kg for state I and II, higher than those proposed by Ochs and co-workers (Fig. 9). The same evidence is reported by different authors when studying the uptake of Ra by cements with different compositions. For example, Bayliss et al. (2000) studied OPC and blended cements with 75 wt% of BFS; they obtained relatively high distribution

Table 4
Analyses of the aqueous and solid fractions of the synthetized C-A-S-H gels.

	Aqueous				*Solid*			
C-A-S-H (Ca/Si − Al/Si ratio) sample 10 g/L	*Ca (M)*	*Si (M)*	*Al (M)*	*pH*	*Ca/Si (XRF)*	*Al/Si (XRF)*	*Ca/(Al + Si) (XRF)*	*ζ-potential (mV)*
C-A-S-H (0.8–0.05)	5.99×10^{-3}	8.19×10^{-4}	$< 1.11 \times 10^{-6}$	10.20	0.636	0.045	0.609	−11.3 ± 0.7
C-A-S-H (0.8–0.20)	1.32×10^{-2}	1.64×10^{-3}	$< 1.11 \times 10^{-6}$	10.40	0.477	0.189	0.402	−21.4 ± 0.9
C-A-S-H (1.2–0.05)	6.99×10^{-3}	7.48×10^{-5}	1.00×10^{-5}	11.40	0.933	0.047	0.891	9.3 ± 0.6
C-A-S-H (1.2–0.20)	1.40×10^{-2}	2.21×10^{-4}	5.19×10^{-5}	11.00	0.778	0.184	0.657	−1.2 ± 0.5

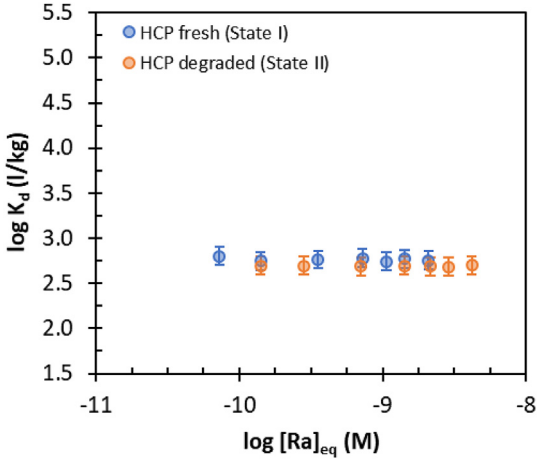

Fig. 4. Adsorption isotherms of Ra ($[Ra]_0 = 8.0 \times 10^{-10} - 2.5 \times 10^{-8}$ M) on the HCP samples (States I and II).

Table 5
Summary of the system pH values, Ca concentrations, and K_d values obtained from the adsorption experiments carried out in this study.

Sample	S/L	pH	[Ca]	Mean log K_d
	(g/L)		(mol/L)	(L/kg)
Sound HCP (St. I)	10	13.20	1.05×10^{-3}	2.77 ± 0.02
Degraded HCP (St. II)	10	12.20	4.74×10^{-3}	2.69 ± 0.01
C-S-H (0.8)	20			4.14 ± 0.13
C-S-H (0.8)	10	10.38	1.10×10^{-3}	4.17 ± 0.11
C-S-H (1.0)	10	11.41	2.05×10^{-3}	3.85 ± 0.08
C-S-H (1.2)	10	12.19	5.09×10^{-3}	3.76 ± 0.07
C-S-H (1.6)	10	12.37	1.50×10^{-2}	2.75 ± 0.04
C-A-S-H (0.8–0.05)	10	10.20	5.99×10^{-3}	3.95 ± 0.06
C-A-S-H (0.8–0.20)	10	10.40	1.32×10^{-2}	4.34 ± 0.09
C-A-S-H (1.2–0.05)	10	11.40	6.99×10^{-3}	3.97 ± 0.05
C-A-S-H (1.2–0.20)	10	11.00	1.40×10^{-2}	5.11 ± 0.12

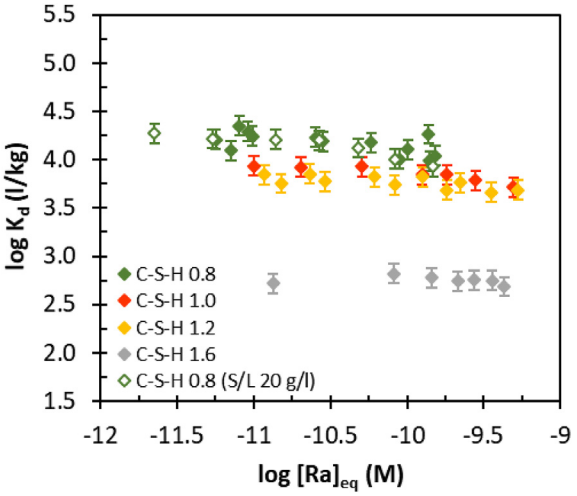

Fig. 5. Adsorption isotherms of Ra on C-S-H phases (for the Ca/Si = 0.8 sample, solid and open squares stand for S/L ratios of 10 and 20 g/L, respectively).

ratios for the OPC/BFS blend, which was attributed to the formation of $RaSO_4$. More recently, Lange et al. (2018) observed a higher retention potential of the blended HCP made with 30 wt% BFS and 40 wt% SF compared to that of OPC. The use of supplementary cementitious materials (SCM) in cement reportedly leads to a decrease in the portlandite content; it also promotes the formation of C-S-H gels with low Ca/Si

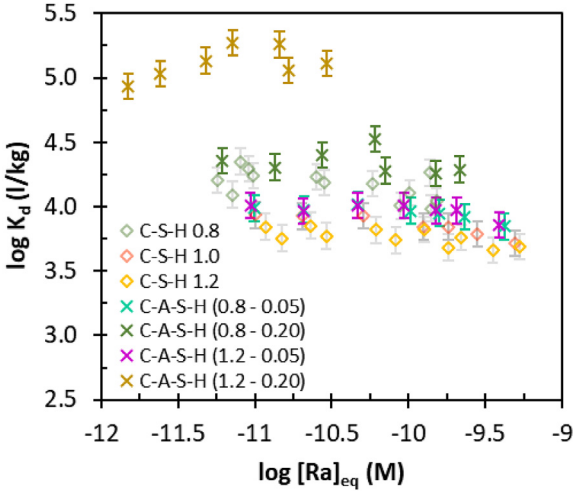

Fig. 6. Adsorption isotherms of Ra on C-A-S-H phases (S/L = 10 g/L). Results from C-S-H 0.8 (S/L 10 g/L); 1.0 and 1.2 have been also included for comparison.

ratios (Massazza, 1993; Lothenbach et al., 2011), which, in turn, increases the retention properties compared to those of OPC.

Tits et al. (2006a) investigated the adsorption of Ra on C-S-H phases with variable Ca/Si ratios in fresh (pH = 13.3) and degraded (pH = 12.5) pore solutions. They observed higher adsorption in fresh (~20,000–~800 L/kg) than in degraded (~2,000–~100 L/kg) pore waters (Fig. 9), with the Ra uptake decreasing as the Ca/Si ratio increases. The same trend was observed by Lange et al. (2018), who studied C-S-H phases with Ca/Si ratios of 0.9 and 1.4 in different pore waters (pH = 13.3 and ~12). However, they reported a significant reduction in Ra uptake due to the presence of alkalis (~13,000–~950 L/kg), compared to the Ra uptake in the alkali-free solution (~23,000–~1800 L/kg); this reduction was attributed to (i) alkalis taking part as competing cations, (ii) changes in the C-S-H surface charge, and (iii) formation of $RaOH^+$ species (Fig. 9). The distribution coefficients obtained here are comparable to those reported by these authors in fresh waters (~14,700 to ~560 L/kg); they are higher than those reported by Tits et al. (2006a), at equal Ca concentrations (Figs. 8 and 9). The adsorption data of Ra on C-S-H is systematically stronger than that of Ba on these phases (Missana et al., 2017). Therefore, the traditional assumption of the Ba-Ra analogy must be considered conservative.

The effects of the S/L ratios used in the batch tests were studied by Tits et al. (2006a) and Lange et al. (2018), from 0.1 to 10 g/L and from 5 to 10 g/L, respectively. For S/L ratios below 40 g/L, no significant influence was observed by Lange et al. (2018) on the obtained K_d within the limits of the initial Ra concentration investigated (8×10^{-10} - 2.5×10^{-8} M). This is consistent with the results obtained in this work, where the differences in the K_d values between the two S/L ratios studied (10 and 20 g/L) were within the range of uncertainty (Table 5).

Ra adsorption onto the C-A-S-H gels was found to be fast with K_d values ranging from 1.3×10^5 to 8.9×10^3 L/kg (Fig. 9). The retention capacities of these phases depend on the initial amount of Al present in the system; the capacities increase with the Al concentrations in the systems. As far as the authors know, there are no studies related to Ra adsorption onto this type of cement hydrates. Studies on Cs, Sr, and alkali adsorption onto C-A-S-H gels (Li and Pang, 2014; Hong and Glasser, 2002) indicate an enhancement of the uptake compared to those of C-S-H phases, due to Si substitution by tetrahedral Al in the bridging position, which induces (i) charge compensation mechanisms, and (ii) the polymerization of dreierketten chains that promotes supplementary surface sites for adsorption (Sun et al., 2006; L'Hôpital et al., 2015; Li and Pang, 2014; Hong and Glasser, 2002). Comparing

Table 6
Reactions and parameters used for Ra adsorption modelling on C-S-H phases.

Description	Reaction	Log K	Density (μmol/m^2)
Silanol (weak site)	$SiOH \Leftrightarrow SiO^- + H^+$	6.80 ± 0.5 (Papirer, 2000)	13 (Missana et al., 2017)
Silanol (strong site)	$Si_sOH \Leftrightarrow Si_sO^- + H^+$	6.80 ± 0.5 (Papirer, 2000)	0.0035 (Missana et al., 2017)
Exchange site	X_2Ca	–	2 (Missana et al., 2017)
Ca Complexation (C-S-H charge)	$SiO^- + Ca^{2+} \Leftrightarrow SiOCa^+$	−4.12 (Missana et al., 2017)	
Description	**Reaction**	**Ba adsorption Log K (Missana et al., 2017)**	**Ra adsorption Log K (this work)**
Complexation of M^{2+} on weak sites	$SiO^- + M^{2+} \Leftrightarrow SiOM^+$	−4.5	−4.5
Complexation of M^{2+} on strong sites	$Si_sO^- + M^{2+} \Leftrightarrow Si_sOM^+$	−0.3	0.3
M^{2+} exchange with Ca^{2+}	$X_2Ca + M^{2+} \Leftrightarrow X_2M + Ca^{2+}$	1.30	1.35

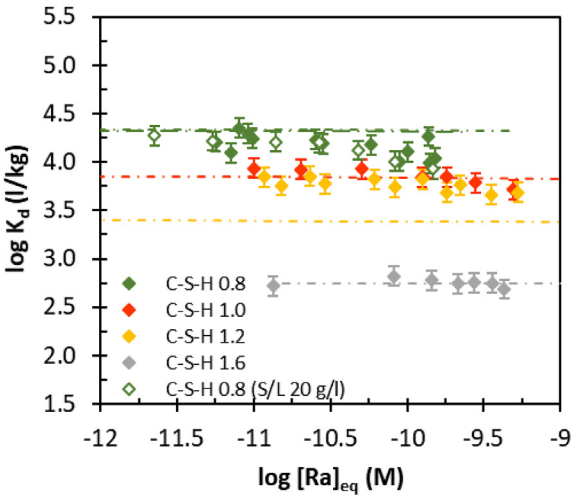

Fig. 7. Adsorption isotherms of Ra on the C-S-H phases and modelling approach of adsorption data. Symbols correspond to experimental data and dashed-dotted lines to model calculations.

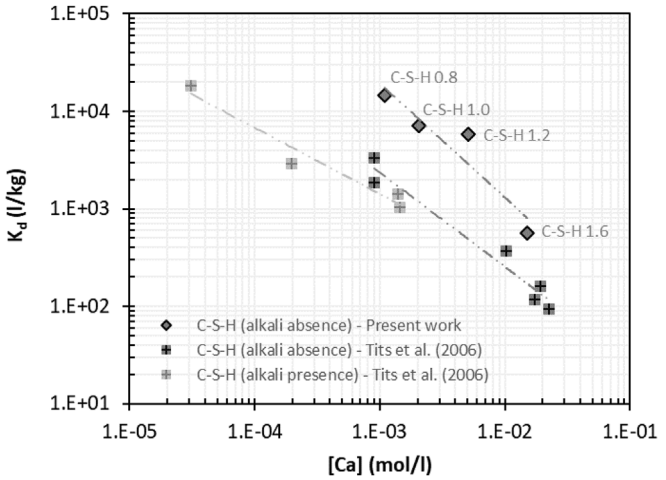

Fig. 8. Evolution of Ra distribution coefficients against Ca concentration in the pore water for the C-S-H gels (dark grey diamonds). Data from Tits et al. (2006a) are included for comparison (dark and light grey squares are C-S-H phases in the absence and presence of alkalis, respectively).

the adsorption capacities of the C-S-H and C-A-S-H samples in this work, the presence of Al slightly influenced the Ra uptake. Some improvements can be observed for the phases with high Ca/Si ratios, although these are not enough to establish a clear pattern.

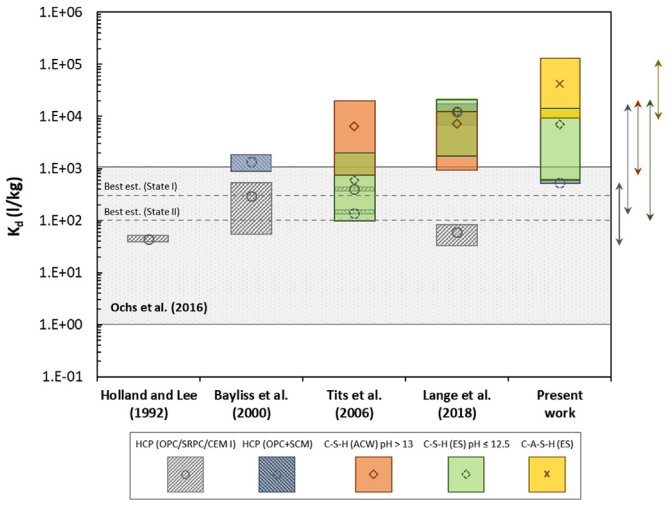

Fig. 9. Summary of compiled K_d values obtained in the present work compared to data reported in the literature (Holland and Lee, 1992; Bayliss et al., 2000; Tits et al., 2006a; Lange et al., 2018) for Ra on HCP and pure phases (C-(A)S-H). Boxes and symbols are respectively the range of experimentally acquired values and the averaged values. Grey boxes and circles stand for the HCP based on ordinary Portland cement (OPC/SRPC/CEM I); dark blue boxes and circles stand for blended HCP, including SCM (OPC + SCM); orange boxes and diamonds stand for C-S-H gels in ACW (ACW pH > 13); green boxes and diamonds stand for C-S-H gels in equilibrium solutions (ES pH ≤ 12.5); yellow box and cross stands for the C-A-S-H gels in equilibrium solutions (ES). Grey area and dashed lines denote upper/lower limits and best estimate K_d values for HCPs at degradation states I and II proposed by Ochs et al. (2016). The arrows at the right side of the plot indicate the range of K_d values obtained for each type of studied system. (For interpretation of the references to colour in this figure legend, the reader is referred to the Web version of this article.)

6. Conclusions

The solutes interacting with the cement phases significantly influence the capacity of Ra adsorption onto hydrated cements. The experiments performed in this work show that the binding of Ra onto the cement phases is slightly higher than that of Ba, and it is interpreted as being driven by surface complexation and ionic exchange processes with Ca.

The results indicate that the C-S-H and C-A-S-H phases are important cementitious hydrates involved in Ra retention. Since Ca is the principal competitor limiting the adsorption of Ra in cementitious materials, an eventual decalcification of cement would lead to improved Ra adsorption capacities of these cement hydrates.

Regarding the C-A-S-H phases, it can be concluded that the incorporation of Al into C-S-H increases the adsorption capacity under the studied conditions for the highest Ca/Si ratios. Studies on the adsorption properties of these cementitious phases are few; fortunately, the

study presented here provides some insight into this matter. Nevertheless, further studies with extensive characterisation (^{29}Si, ^{27}Al-NMR, TGA, SEM-EDX, BET, etc.) are advisable to evaluate the extent of the effect of Al (present in C-A-S-H phases) on Ra adsorption, as well as to establish the mechanism of adsorption taking place in these cement phases. All these studies will help better understand the role and relevance these phases might have in real cementitious systems with respect to radionuclide retention, as well as the effect of using FA/BFS blended cements as engineered barriers for radwaste disposals.

Appendix A. Supplementary data

Supplementary data to this article can be found online at https://doi.org/10.1016/j.apgeochem.2019.04.004.

References

Adenot, F., 1992. Durabilité du béton: Caractérisation et modélisation des processus physiques et chimiques de dégradation du ciment. PhD thesis. Université d'Orléans.

Aggarwal, S., Angus, M., Ketchen, J., 2000. Sorption of Radionuclides onto Specific Mineral Phases Present in Repository Cements. AEA – D&R – 0395. NSS/R312. .

Andersen, M.D., Jakobsen, H.J., Skibsted, J., 2006. A new aluminium-hydrate species in hydrated Portland cements characterized by ^{27}Al and ^{29}Si MAS NMR spectroscopy. Cement Concr. Res. 36, 3–17.

Andra, 2012. The Management of Radioactive Waste Resulting from the Production of Rare Earths or of Groundwaters Loaded with Mineral Salts. Available on. http://www.andra.fr/international/download/andra-international-en/document/4-RadiumBearing.pdf.

Atkins, M., Glasser, F.P., 1992. Application of Portland cement-based materials to radioactive waste immobilization. Waste Manag. 12, 105–131.

Atkins, M., Glasser, F.P., Kindness, A., 1992. Cement hydrate phase: solubility at 25 C. Cement Concr. Res. 22 (2–3), 241–246.

Bach, T., Chabas, E., Pochard, I., Coumes, C.C.D., Haas, J., Frizon, F., Nonat, A., 2013. Retention of alkali ions by hydrated low-pH cements: mechanism and Na^+/K^+ selectivity. Cement Concr. Res. 51, 14–21.

Bayliss, S., Howse, R.M., McCrohon, R., Oliver, P., 2000. Near-field Sorption Studies. AEAT/ERRA-0073 Technical Report. .

Beaudoin, J.J., Ramachandran, V.S., Feldmann, R.F., 1990. Interaction of chloride and C-S-H. Cement Concr. Res. 20, 875–883.

Chen, W., Brouwers, H.J.H., 2010. Alkali binding in hydrated Portland cement paste. Cement Concr. Res. 40 (5), 716–722.

Chen, J.J., Thomas, J.J., Taylor, H.F., Jennings, H.M., 2004. Solubility and structure of calcium silicate hydrate. Cement Concr. Res. 34 (9), 1499–1519.

Cong, X., Kirkpatrick, R.J., 1996. ^{29}Si MAS NMR study of the structure of calcium silicate hydrate. Adv. Cem. Base Mater. 3 (3), 144–156.

Evans, N.D.M., 2008. Binding mechanisms of radionuclides to cement. Cement Concr. Res. 38 (4), 543–553.

Faucon, P., Delagrave, A., Petit, J.C., Richet, C., Marchand, J.M., Zanni, H., 1999. Aluminium incorporation in calcium silicate hydrates (C− S− H) depending on their Ca/Si ratio. J. Phys. Chem. B 103 (37), 7796–7802.

Flint, E.P., Wells, L.S., 1934. Study of the system CaO-SiO_2-H_2O at 30° C and of the reaction of water on the anhydrous calcium silicates. J. Res. Natl. Bur. Stand. 12, 751–783.

Giffaut, E., Grivé, M., Blanc, Ph, Vieillard, Ph, Colàs, E., Gailhanou, H., Gaboreau, S., Marty, N., Madé, B., Duro, L., 2014. Andra thermodynamic database for performance assessment: ThermoChimie. Appl. Geochem. 49, 225–236. https://www.thermochimie-tdb.com.

Glasser, F., Tyrer, M., Quillin, K., 1999. The Chemistry of Blended Cements and Backfills Intended for Use in Radioactive Waste Disposal (No. EA-RD-TR-P–98). Environment Agency.

Grangeon, S., Claret, F., Linard, Y., Chiaberge, C., 2013. X-ray diffraction: a powerful tool to probe and understand the structure of nanocrystalline calcium silicate hydrates. Acta Crystallogr. B: Structural Science, Crystal Engineering and Materials 69 (5), 465–473.

Greenberg, S.A., Chang, T.N., 1965. Investigation of the colloidal hydrated calciumsilicates. II. Solubility relationships in the calcium-silica-water system at 25 °C. J. Phys. Chem. 69, 182–188.

Grutzeck, M., Benesi, A., Fanning, B., 1989. Silicon29 magic angle spinning nuclear magnetic resonance study of calcium silicate hydrates. J. Am. Ceram. Soc. 72 (4), 665–668.

Haas, J., 2012. Etude expérimentale et modélisation thermodynamique du système CaO-SiO_2-(Al_2O_3)-H_2O. Universite de Bourgogne, Dijon, France, pp. 183 2012.

Henocq, P., 2005. Modélisation des interactions ioniques à la surface des silicates de calcium hydratés. L'Universite Laval, Quebec, Canada, pp. 204 2005.

Henocq, P., 2017. A sorption model for alkalis in cement-based materials – correlations with solubility and electrokinetic properties. In: Physics and Chemistry of the Earth, Parts A/B/C Volume 99, June 2017, pp. 184–193.

Holland, T.R., Lee, D.J., 1992. Radionuclide getters in cement. Cement Concr. Res. 22, 247–258.

Hong, S.Y., Glasser, F.P., 1999. Alkali binding in cement pastes. Part I. The C-S-H phases. Cement Concr. Res. 29 (12), 1893–1903.

Hong, S.Y., Glasser, F.P., 2002. Alkali sorption by CSH and CASH gels: Part II. Role of alumina. Cement Concr. Res. 32 (7), 1101–1111.

International Atomic Energy Agency, 2011. Radiation Protection and Safety of Radiation Sources: International Basic Safety Standards – Interim Edition, Safety Standards Series No. GSR Part 3 (Interim). IAEA, Vienna.

Lange, S., Kowalski, P.M., Pšenička, M., Klinkenberg, M., Rohmen, S., Bosbach, D., Deissmann, G., 2018. Uptake of ^{226}Ra in cementitious systems: a complementary solution chemistry and atomistic simulation study. Appl. Geochem. 96, 204–216.

Li, K., Pang, X., 2014. Sorption of radionuclides by cement-based barrier materials. Cement Concr. Res. 65, 52–57.

Lodeiro, I.G., Fernández-Jimenez, A., Palomo, A., Macphee, D.E., 2010. Effect on fresh CSH gels of the simultaneous addition of alkali and aluminium. Cement Concr. Res. 40 (1), 27–32.

Lothenbach, B., Scrivener, K., Hooton, R.D., 2011. Supplementary cementitious materials. Cement Concr. Res. 41 (12), 1244–1256.

L'Hôpital, E., Lothenbach, B., Le Saout, G., Kulik, D., Scrivener, K., 2015. Incorporation of aluminium in calcium-silicate-hydrates. Cement Concr. Res. 75, 91–103.

L´Hôpital, E., Lothenbach, B., Kulik, D.A., Scrivener, K., 2016. Influence of calcium to silica ratio on aluminium uptake in calcium silicate hydrate. Cement Concr. Res. 85, 111–121.

Massazza, F., 1993. Pozzolanic cements. Cement Concr. Compos. 15 (4), 185–214.

Missana, T., García-Gutiérrez, M., Mingarro, M., Alonso, U., 2017. Analysis of barium retention mechanisms on calcium silicate hydrate phases. Cement Concr. Res. 93, 8–16.

Ochs, M., Pointeau, I., Giffaut, E., 2006. Caesium sorption by hydrated cement as a function of degradation state: experiments and modelling. Waste Manag. 26 (7), 725–732.

Ochs, M., Mallants, D., Wang, L., 2016. Radionuclide and Metal Sorption on Cement and Concrete. Springer International Publishing.

Olmeda, J., Henocq, P., Giffaut, E., Grivé, M., 2017. Modelling of chemical degradation of blended cement-based materials by leaching cycles with Callovo-Oxfordian pore-water. Phys. Chem. Earth, Parts A/B/C 99, 110–120.

Papadokostaki, K.G., Savidou, A., 2009. Study of leaching mechanisms of caesium ions incorporated in Ordinary Portland Cement. J. Hazard Mater. 171 (1–3), 1024–1031.

Papirer, E., 2000. Adsorption on Silica Surfaces. Marcel Dekker, NY 2000 13:978-0824700034.

Pardal, X., Pochard, I., Nonat, A., 2009. Experimental study of Si–Al substitution in calcium-silicate-hydrate (CSH) prepared under equilibrium conditions. Cement Concr. Res. 39 (8), 637–643.

Pardal, X., Brunet, F., Charpentier, T., Pochard, I., Nonat, A., 2012. Al-27 and Si-29 solid-state NMR characterization of calcium-aluminosilicate-hydrate. Inorg. Chem. 51 (3), 1827–1836.

Parkhurst, D.L., Appelo, C.A.J., 2013. Description of input and examples for PHREEQC version 3: a computer program for speciation, batch-reaction, one-dimensional transport, and inverse geochemical calculations (No. 6-A43). In: US Geological Survey. Techniques and Methods, book 6, chap. A43, pp. 497.

Pointeau, I., 2000. Etude mécanistique et modelisation de la retention de radionucléides par les silicates de calcium hydrates (CSH) des cimets. Thése Université de Reims Champagne-Ardenne. Collection Les Rapports (ANDRA).

Pointeau, I., Marmier, N., Fromage, F., Fedoroff, M., Giffaut, E., 2001. Caesium and lead uptake by CSH phases of hydrated cement. MRS Online Proceedings Library Archive 663, 105–113.

Pointeau, I., Landesman, C., Giffaut, E., Reiller, P., 2004. Reproducibility of the uptake of U (VI) onto degraded cement pastes and calcium silicate hydrate phases. Radiochim. Acta 92 (9–11), 645–650.

Pointeau, I., Reiller, P., Macé, N., Landesman, C., Coreau, N., 2006. Measurement and modeling of the surface potential evolution of hydrated cement pastes as a function of degradation. J. Colloid Interface Sci. 300 (1), 33–44.

Renaudin, G., Russias, J., Leroux, F., Cau-dit-Coumes, C., Frizon, F., 2009. Structural characterization of C-S-H and C-A-S-H samples-Part II: local environment investigated by spectroscopic analyses. J. Solid State Chem. 182 (12), 3320–3329.

Richardson, I.G., Groves, G.W., 1993. Models for the composition and structure of Calcium Silicate Hydrate (C-S-H) gel in hardened tricalcium silicate pastes and the incorporation of minor and trace-elements into Calcium Silicate Hydrate (C-S-H) gel in hardened cement pastes - Reply. Cement Concr. Res. 23, 999–1000.

Roosz, C., Vieillard, P., Blanc, P., Gaboreau, S., Gailhanou, H., Braithwaite, D., Madé, B., 2018. Thermodynamic properties of CSH, CASH and MSH phases: results from direct measurements and predictive modelling. Appl. Geochem. 92, 140–156.

Sugiyama, D., 2008. Chemical alteration of calcium silicate hydrate (C–S–H) in sodium chloride solution. Cement Concr. Res. 38 (11), 1270–1275.

Sun, G.K., Young, J.F., Kirkpatrick, R.J., 2006. The role of Al in C-S-H: NMR, XRD, and compositional results for precipitated samples. Cement Concr. Res. 36 (1), 18–29 2006.

Taylor, H.W., 1950. 726. Hydrated calcium silicates. Part I. Compound formation at ordinary temperatures. J. Chem. Soc. 3682–3690.

Taylor, H.F.W., 1997. Cement Chemistry. Thomas Telford, pp. 459.

Tits, J., Iijima, K., Wieland, E., Kamei, G., 2006a. The uptake of radium by calcium silicate hydrates and hardened cement paste. Radiochim. Acta 94, 637–643.

Tits, J., Wieland, E., Müller, C.J., Landesman, C., Bradbury, M.H., 2006b. Strontium binding by calcium silicate hydrates. J. Colloid Interface Sci. 300 (1), 78–87.

Tournassat, C., Grangeon, S., Leroy, P., Giffaut, E., 2013. Modeling specific pH dependent sorption of divalent metals on montmorillonite surfaces. A review of pitfalls, recent achievements and current challenges. Am. J. Sci. 313 (5), 395–451.

Trapote-Barreira, A., Cama, J., Soler, J.M., 2014. Dissolution kinetics of C–S–H gel: flow-through experiments. Phys. Chem. Earth, Parts A/B/C 70, 17–31.

Viallis-Terrisse, H., 2000. Interaction des Silicates de Calcium Hydratés, principaux constituants du ciment, avec les chlorures d'alcalins. Analogie avec les argiles. These de Doctorat. Universite de Bourgogne.
Viallis-Terrisse, H., Nonat, A., Petit, J.C., 2001. Zeta-potential study of calcium silicate hydrates interacting with alkaline cations. J. Colloid Interface Sci. 244 (1), 58–65.
Walker, C.S., Savage, D., Tyrer, M., Ragnarsdottir, K.V., 2007. Non-ideal solid solution aqueous solution modeling of synthetic calcium silicate hydrate. Cement Concr. Res. 37 (4), 502–511.
Walker, C.S., Sutou, S., Oda, C., Mihara, M., Honda, A., 2016. Calcium silicate hydrate (CSH) gel solubility data and a discrete solid phase model at 25° C based on two binary non-ideal solid solutions. Cement Concr. Res. 79, 1–30.
Wang, L., Jacques, D., De Cannière, P., 2010. Effects of an Alkaline Plume on the Boom Clay as a Potential Host Formation for Geological Disposal of Radioactive Waste. External Report SCK-CEN-ER-28. SCK-CEN, Belgium.